Supporting Material

Effects of Inorganic Salts on the Heterogeneous OH Kinetic and Chemistry of Organic Compounds: Insights from Methylglutaric Acid-Ammonium Sulfate

Hoi Ki Lam[1], Sze Man Shum[1], James F. Davies[2], Mijung Song[3], Andreas Zuend[4], and Man Nin Chan[1,5]

[1]Earth System Science Programme, Faculty of Science, The Chinese University of Hong Kong, Hong Kong, China
[2]Department of Chemistry, University of California Riverside, Riverside, CA, USA
[3]Department of Earth and Environmental Sciences, Chonbuk National University, Jeollabuk-do, Republic of Korea
[4]Department of Atmospheric and Oceanic Sciences, McGill University, Montreal, Québec, Canada
[5]The Institute of Environment, Energy, and Sustainability, The Chinese University of Hong Kong, Hong Kong, China

Phase separation measurement of 3-MGA-AS particles in OIR = 2

To investigate the phase separation behavior, the 3-MGA-AS solution was first prepared by dissolving 3-MGA and AS in deionized water with an OIR of 2. **Figure S1** shows a schematic diagram of the experimental setup for the phase separation measurements. Micrometer-sized aqueous droplets of 3-MGA-AS (26.3–38.5 μm in diameter) were generated and deposited onto a hydrophobically coated substrate (Hampton Research; 22mm × 0.96mm Thick Siliconized Square Cover Slides) using a droplet generator (MicroFab; JetDrive™ III Controller). The substrate was then mounted on a sample holder inside an aerosol flow cell (Parsons et al., 2004; Pant et al., 2006; Song et al., 2012a). The size and morphology of particles were monitored by an optical microscope (Nikon; long working distance 20X objective) with an electronic eyepiece camera (Ningbo Hi-Tech; EHB Series C-mount USB2.0 CMOS Eyepiece Camera) as a function of RH. A continuous flow of dry and humidified N_2 mixture was introduced into the cell with a flow rate of 0.5 L min^{-1} to control the RH inside the flow cell by adjusting the mixing ratio of dry and humidified N_2. A RH sensor was used to measure the RH inside the cell and was calibrated by measuring the deliquescence relative humidity (DRH) of AS (DRH = 80.0 %), sodium chloride (DRH = 75.0 %) and ammonium nitrate (DRH = 65.5 %) at 20 ℃ (Martin, 2000). After calibration, the uncertainty of the RH was ± 2.7 %.

In a typical experiment at 21℃, the RH inside the aerosol flow cell was initially set at about 90 %. After equilibrium, the size and morphology of the droplets were recorded. We then dropped stepwise the RH by about 1–3% and waited for 5–10 minutes for the RH to stabilize before taking a new record. The lowest RH to be investigated was around 40 %, at which AS typically crystallizes. Since the RH was varied in discrete steps, the separation RH (SRH) was recorded and reported as a range, with the RH before the occurrence of phase separation as the upper boundary and the first RH with the observed onset of phase separation as the lower boundary.

Phase separation of 3-MGA-AS particles

Figure S2 shows the morphological features of a micrometer-sized 3-MGA-AS particles with diameter of 38.5 μm in an OIR of 2 upon dehumidification. At RH ≥ 73.6 %, the particles exhibits a single liquid phase. The onset of liquid-liquid phase separation upon dehumidification occurs between 72.7–73.6 % RH, indicated by the appearance of small inclusions in the particle, which

likely contains AS and water. As RH further decreases, these satellite inclusions coalesce to form larger inclusions. Although there is no direct observation of schlieren (at the present optical magnification), a highly inter-connective structure, we postulate that the mechanism of phase separation in the 3-MGA-AS particles could be spinodal decomposition. It might be partly supported by the vast amount of small inclusions in the droplet observed at the onset of phase separation which is a likely feature of spinodal decomposition due to the absence of energy barrier, in contrast to nucleation and growth, which typically only takes place at a few isolated nucleation sites (Ciobanu et al., 2009). However, more work is required to verify the mechanism tentatively proposed here.

We acknowledge that the phase separation of submicron-sized 3-MGA-AS particles investigated in this work has not been studied. Recently, O'Brien et al. (2015) have observed the occurrence of phase separation in smaller micrometer-sized particles (~1 μm in diameter) using an environmental scanning electron microscope and a scanning transmission X-ray microscope. The SRH of PEG-400-AS and α,-dihydroxy-3-methoxybenzeneaceticacid-AS particles reported in their work are consistent with the results for larger droplets (> 20 μm). These results are consistent with the work of Krieger et al. (2012), which suggests that the phase separation behavior is not affected by the particle size, as long as the Kelvin effect is not significant. Moreover, aerosol modelling studies have indicated a potential size dependence of SRH and mechanism in nanosized particles, partially due to the fast experimental drying rates employed, yet with phase separation by spinodal decomposition observed down to small particles with diameter of a few tens of nanometer (Altaf et al., 2016; Altaf and Freedman 2017). In this work, the size of the particles before oxidation was about 200 nm in diameter. The phase separation behavior observed in micrometer-sized particles could provide a good first approximation. Furthermore, since the particles were always exposed to high humidity and the experiments were carried out at 85.0 % RH, which is higher than the SRH (72.7–73.6 % RH, **Table 1**), 3-MGA-AS particles are likely to be single-phase liquid droplets prior to oxidation.

Simple analysis on the surface coverage of 3-MGA in 3-MGA and 3-MGA-AS particles

In this section, we attempt to roughly estimate the surface coverage of 3-MGA in 3-MGA and 3-MGA-AS particles. By assuming that all species within the particles are well mixed and acquire

spherical shapes (i.e. cross-sectional surface area of each species is directly proportional to the square of their molecular radius), the surface coverage (θi) of a species can be roughly estimated using a simple additive rule as shown below:

$$\theta i = \frac{n_i \times r_i{}^2}{\sum n_i \times r_i{}^2} \qquad \text{(Eqn. S1)}$$

where n_i is the mole fraction of the species i, and r_i is the effective radius of each molecule of species i. The mole fraction of the species can be deduced from dividing its mass concentration (e.g. *mfs*) by its molecular weight. Further, using the molecular weight and density data, the effective radii of water and 3-MGA are estimated to be 0.193 nm and 0.364 nm, respectively. The effective radii of ammonium and sulfate ions are reported to be 0.143 and 0.242 nm, respectively (Masterton et al., 1971; Marcus, 1988). Using these parameters and Eqn. S1, the surface coverage of 3-MGA in 3-MGA particles and 3-MGA-AS particles are estimated to be 51.4% and 21.6%, respectively. This supports our hypothesis that a lower surface coverage of 3-MGA in 3-MGA-AS particles might reduce the collision probability between 3-MGA and gas-phase OH radicals at the gas/particle interface and lower the overall heterogeneous reactivity compared to 3-MGA particles.

Change in the average elemental composition upon oxidation

If we assume that the identified products could well represent the overall particle composition, with the relative abundances and molecular information of the reaction products, the average elemental composition of the particles can be computed, assuming the ionization efficiency of the 3-MGA and reaction products are the same as a first approximation. The average oxygen-to-carbon ratio ($\langle O/C \rangle$) and hydrogen-to-carbon ratio ($\langle H/C \rangle$) of the organic fraction can be obtained as follows (Chan et al., 2014),

$$\langle O/C \rangle = \frac{\sum_i (O/C)_i\, n_{C,i}\, I_i}{\sum_i n_{C,i}\, I_i} = \frac{\sum_i n_{O,i}\, I_i}{\sum_i n_{C,i}\, I_i} \quad \text{(Eqn. S2)}$$

$$\langle H/C \rangle = \frac{\sum_i (H/C)_i\, n_{C,i}\, I_i}{\sum_i n_{C,i}\, I_i} = \frac{\sum_i n_{H,i}\, I_i}{\sum_i n_{C,i}\, I_i} \quad \text{(Eqn. S3)}$$

where $(O/C)_i$, $(H/C)_i$, and I_i are the O/C, H/C and relative abundance of species i, respectively and $n_{C,i}$, $n_{O,i}$, $n_{H,i}$ are the number of carbon atoms, oxyg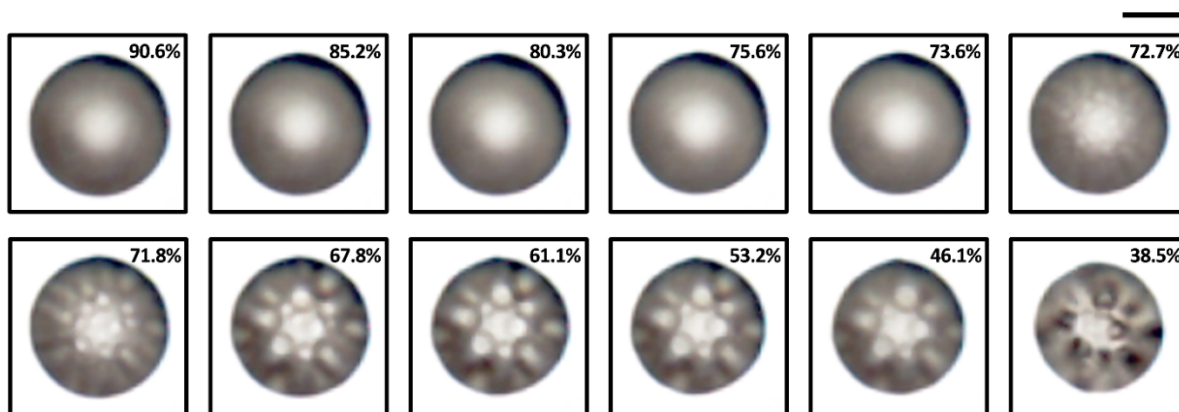en atoms and hydrogen atoms respectively. **Figure S4** shows a van Krevelen diagram for the heterogeneous OH oxidation of 3-MGA and 3-MGA-AS particles as a function of OH exposure. In both systems, as OH exposure increases, $\langle H/C \rangle$ decreases from 1.67 to ~1.63 while $\langle O/C \rangle$ increases from 0.67 to ~0.75–0.77. The slope of

3-MGA-AS and 3-MGA are almost the same, of value –0.39, mainly resulting from a combination of C_6 hydroxyl products (slope = 0) and C_6 ketone products (slope = –2), with the dominance of C_6 hydroxyl products.
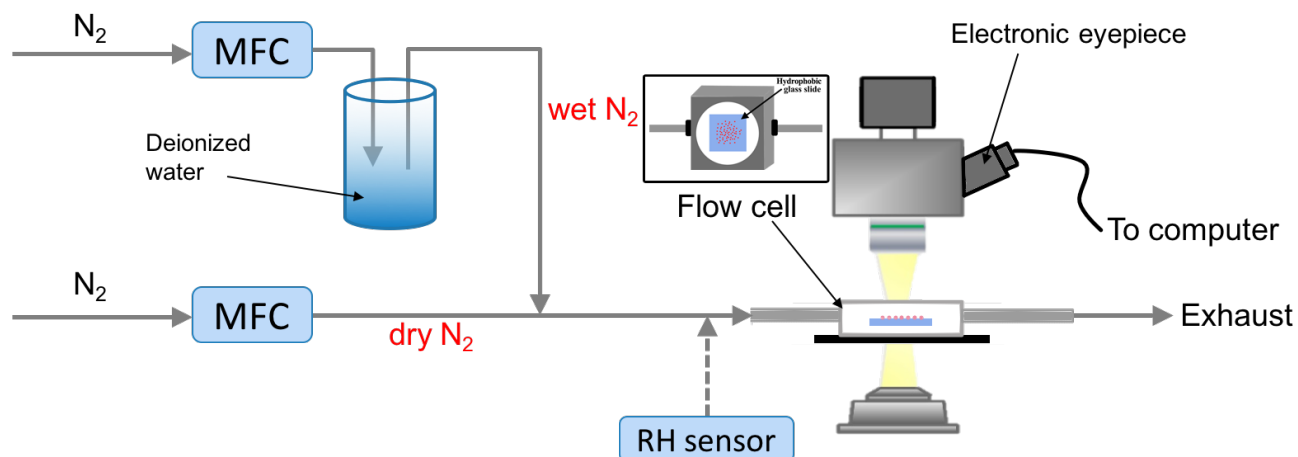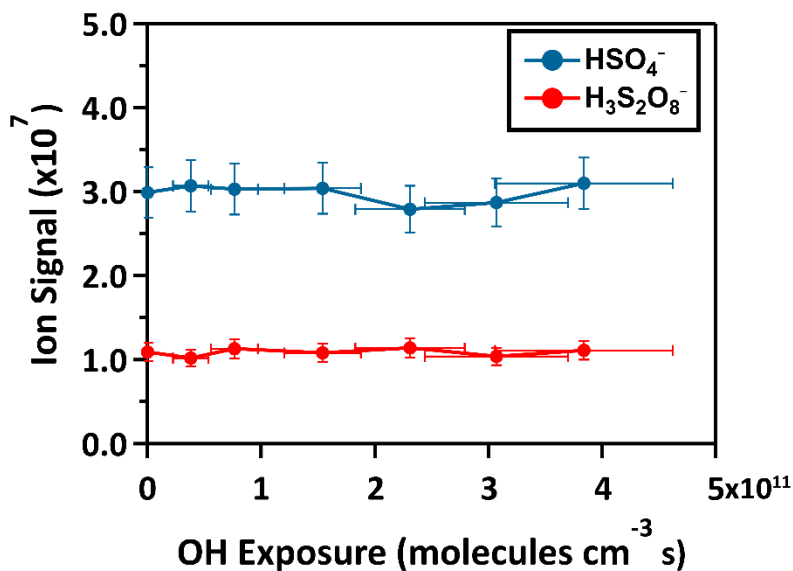

5

Figure S1. A schematic diagram of the experimental setup for phase separation measurement of 3-MGA-AS particles.
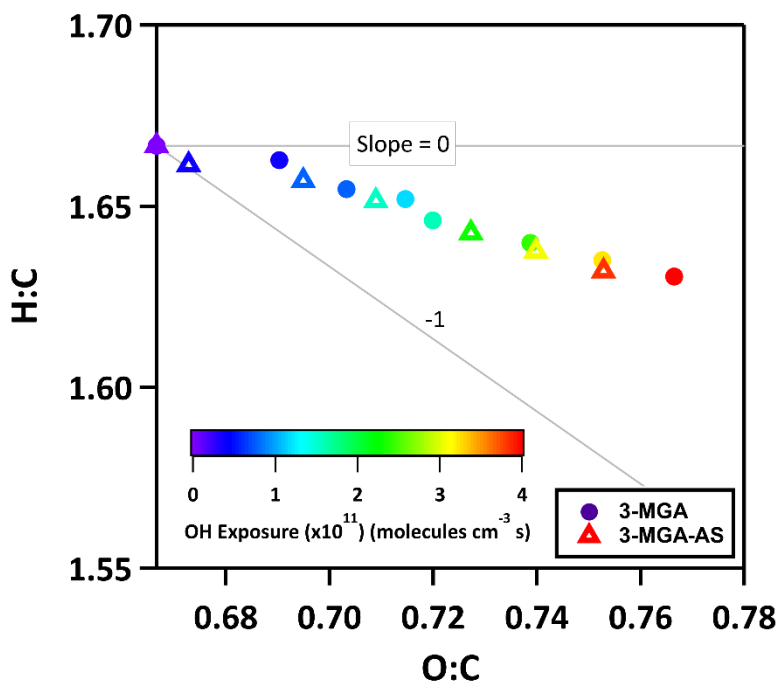

10

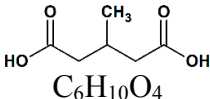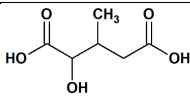**Figure S2.** Morphologies of 3-MGA-AS particles (OIR = 2) upon dehumidification at 21 °C. The size bar at the upper right corner of the figure corresponds to 20 μm.
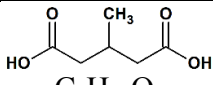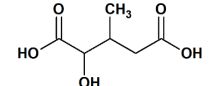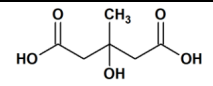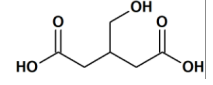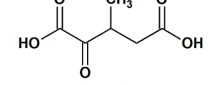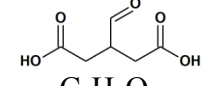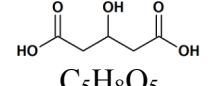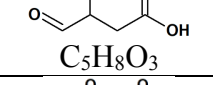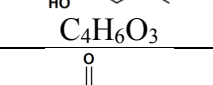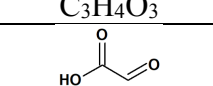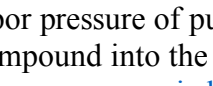
Figure S3. The intensity of inorganic ions detected in 3-MGA-AS particles as a function of OH exposure.

5

10   **Figure S4.** Van Krevelen diagram for the heterogeneous OH oxidation of 3-MGA and 3-MGA-AS particles as a function of OH exposure at 85.0 % RH.
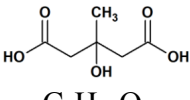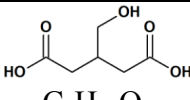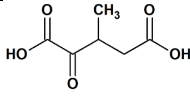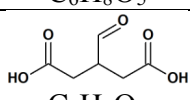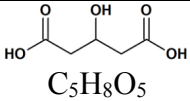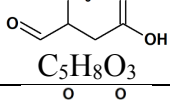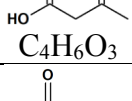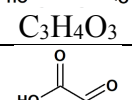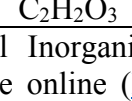
Table S1. SMILES string and vapor pressure of 3-MGA, functionalization products and fragmentation products.

Chemical Structure and Formula	SMILES	Vapor pressure of pure compound (Pa) at 293 K
Parent 3-MGA		
$C_6H_{10}O_4$	CC(CC(=O)O)CC(=O)O	2.49E-04
Functionalization Products		
$C_6H_{10}O_5$	CC(CC(=O)O)C(O)C(=O)O	1.49E-06
$C_6H_{10}O_5$	CC(O)(CC(=O)O)CC(=O)O	5.18E-06
$C_6H_{10}O_5$	O=C(O)CC(CO)CC(=O)O	2.31E-07
$C_6H_8O_5$	CC(CC(=O)O)C(=O)C(=O)O	7.14E-05
$C_6H_8O_5$	O=CC(CC(=O)O)CC(=O)O	1.47E-05
Fragmentation Products		
$C_5H_8O_5$	O=C(O)CC(O)CC(=O)O	2.16E-06
$C_5H_8O_3$	CC(C=O)CC(=O)O	9.48E-01
$C_4H_6O_3$	CC(=O)CC(=O)O	1.87E+00
$C_3H_4O_3$	O=CCC(=O)O	5.91E+00
$C_2H_2O_3$	O=CC(=O)O	1.24E+02

The vapor pressure of pure organic compounds is computed by inputting the SMILES string of each compound into the EVAPORATION model

5   (http://tropo.aeronomie.be/models/evaporation_run.htm).

Table S2. Mass fraction, mole-fraction-based activity coefficient and C* of each organic compound in the presence of water at 85.0 % RH.
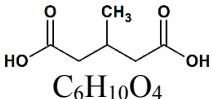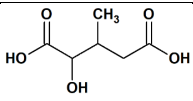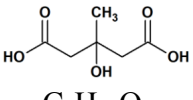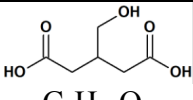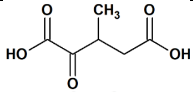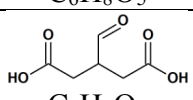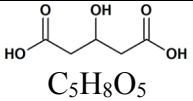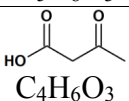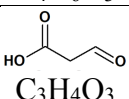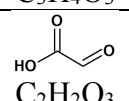
Chemical Structure and Formula	Mass fraction	Activity coefficient [a]	C* ($\mu g/m^3$)
Parent 3-MGA			
$C_6H_{10}O_4$	7.07E-01	7.43E-01	3.60E+00
Functionalization Products			
$C_6H_{10}O_5$	6.27E-01	4.15E-01	1.04E-02
$C_6H_{10}O_5$	6.36E-01	4.54E-01	4.00E-02
$C_6H_{10}O_5$	6.07E-01	3.46E-01	1.28E-03
$C_6H_8O_5$	6.61E-01	5.45E-01	6.96E-01
$C_6H_8O_5$	6.47E-01	5.45E-01	1.39E-01
Fragmentation Products			
$C_5H_8O_5$	5.71E-01	3.59E-01	1.15E-02
$C_5H_8O_3$	7.23E-01	9.88E-01	1.78E+04
$C_4H_6O_3$	6.35E-01	9.61E-01	2.78E+04
$C_3H_4O_3$	5.15E-01	9.00E-01	6.66E+04
$C_2H_2O_3$	4.37E-01	8.33E-01	1.14E+06

[a]Aerosol Inorganic-Organic Mixtures Functional groups Activity Coefficients (AIOMFAC) available online (http://www.aiomfac.caltech.edu or https://aiomfac.lab.mcgill.ca) was used to compute the mass fraction at 85.0 % RH and the activity coefficient of each compound, assuming aqueous droplets (single phase). As $C_6H_8O_5$ formed from the oxidation at secondary carbon site cannot be input into the AIOMFAC, the subgroup with one extra H on the ketone group was input as a proxy to obtain the activity coefficient.

Table S3. Mass fraction, mole-fraction-based activity coefficient and C* of each organic compound in the presence of AS and water with OIR = 2 at 85.0 % RH.
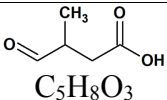
Chemical Structure and Formula	Mass fraction	Activity coefficient	C* ($\mu g/m^3$)
Parent 3-MGA			
$C_6H_{10}O_4$	3.44E-01	1.80E+00	4.73E+00
Functionalization Products			
$C_6H_{10}O_5$	3.24E-01	6.64E-01	1.03E-02
$C_6H_{10}O_5$	3.35E-01	7.25E-01	3.95E-02
$C_6H_{10}O_5$	3.25E-01	5.26E-01	1.26E-03
$C_6H_8O_5$	3.30E-01	9.92E-01	7.40E-01
$C_6H_8O_5$	3.30E-01	9.92E-01	1.52E-01
Fragmentation Products			
$C_5H_8O_5$	3.20E-01	4.52E-01	1.00E-02
$C_5H_8O_3$	3.28E-01	3.09E+00	2.99E+04
$C_4H_6O_3$	3.09E-01	2.13E+00	3.94E+04
$C_3H_4O_3$	2.91E-01	1.27E+00	7.21E+04
$C_2H_2O_3$	2.72E-01	9.72E-01	1.12E+06

5

References

1. Altaf, M. B. and Freedman, M. A.: Effect of drying rate on aerosol particle morphology, J. Phys. Chem. Lett., 8, 3613–3618, 2017.

2. Altaf, M.B, Zuend, A., and Freedman, F. A.: Role of nucleation mechanism on the size dependent morphology of organic aerosol, Chem. Commun., 52, 9220–9223, 2016.

3. Bertram, A. K., Martin, S. T., Hanna, S. J., Smith, M. L., Bodsworth, A., Chen, Q., Kuwata, M., Liu, A., You, Y., and Zorn, S. R.: Predicting the relative humidities of liquid-liquid phase separation, efflorescence, and deliquescence of mixed particles of ammonium sulfate, organic material, and water using the organic-to-sulfate mass ratio of the particle and the oxygen-to-carbon elemental ratio of the organic component, Atmos. Chem. Phys., 11, 10995–11006, 2011.

4. Ciobanu, V. G., Marcolli, C., Krieger, U. K., Weers, U., and Peter, T.: Liquid-liquid phase separation in mixed organic/inorganic aerosol particles, J. Phys. Chem. A, 113, 10966–10978, 2009.

5. Krieger, U. K., Marcolli, C., and Reid, J. P.: Exploring the complexity of aerosol particle properties and processes using single particle techniques, Chem. Soc. Rev., 41, 6631–6662, 2012.

6. Marcus, Y.: Ionic radii in aqueous solutions, Chem. Rev., 88, 1475–1498, 1988.

7. Martin, S. T.: Phase transitions of aqueous atmospheric particles, Chem. Rev., 100, 3403–3453, 2000.

8. Masterton, W. L., Bolocofsky, D., and Lee, T. P.: Ionic radii from scaled particle theory of the salt effect, J. Phys. Chem., 75, 2809–2815, 1971.

9. O'Brien, R. E., Wang, B., Kelly, S. T., Lundt, N., You, Y., Bertram, A. K., Leone, S. R., Laskin, A., and Gilles, M. K.: Liquid-liquid phase separation in aerosol particles: Imaging at the nanometer scale, Environ. Sci. Technol., 49, 4995–5002, 2015.

10. Pant, A., Parsons, M. T., and Bertram, A. K.: Crystallization of aqueous ammonium sulfate particles internally mixed with soot and kaolinite: Crystallization relative humidities and nucleation rates, J. Phys. Chem. A, 110, 8701–8709, 2006.

11. Parsons, M. T., Mak, J., Lipetz, S. R., and Bertram, A. K.: Deliquescence of malonic, succinic, glutaric, and adipic acid particles, J. Geophys. Res.-Atmos., 109, D06212, 2004.

12. Song, M., Marcolli, C., Krieger, U. K., Zuend, A., and Peter, T.: Liquid-liquid phase

separation and morphology of internally mixed dicarboxylic acids/ammonium sulfate/water particles, Atmos. Chem. Phys., 12, 2691–2712, 2012a.

13. Song, M., Marcolli, C., Krieger, U. K., Zuend, A., and Peter, T.: Liquid-liquid phase separation in aerosol particles: Dependence on O:C, organic functionalities, and compositional complexity, Geophys. Res. Lett., 39, L19801, 2012b.

14. You, Y., Renbaum-Wolff, L., and Bertram, A. K.: Liquid–liquid phase separation in particles containing organics mixed with ammonium sulfate, ammonium bisulfate, ammonium nitrate or sodium chloride, Atmos. Chem. Phys., 13, 11723–11734, 2013.

15. You, Y., Smith, M. L., Song, M., Martin, S. T., and Bertram, A. K.: Liquid–liquid phase separation in atmospherically relevant particles consisting of organic species and inorganic salts, Int. Rev. Phys. Chem., 33, 43–77, 2014.